

# Experimental hydraulic fracturing of Berea sandstone under triaxial stress state

Hazem Mubarak<sup>1</sup>, Roshan Saji<sup>1</sup>, Goulong Zhu<sup>2</sup>, Rita Sousa<sup>3</sup>, Mohamed Sassi<sup>2</sup>, and Rashid K. Abu Al-Rub<sup>1,\*</sup>

<sup>1</sup>Department of Mechanical Engineering, Khalifa University of Science and Technology, P.O.Box 127788, Abu Dhabi, United Arab Emirates

<sup>2</sup>Department of Civil Infrastructure and Environmental Engineering, Khalifa University of Science and Technology, P.O.Box 127788, Abu Dhabi, United Arab Emirates

<sup>3</sup>Department of Civil, Environmental and Ocean Engineering, Stevens Institute of Technology, Hoboken, New Jersey, United States of America

**Abstract.** In this work, a newly designed experimental setup is used to perform in-lab fracking under controlled triaxial loading on cylindrical cores of Berea sandstone. Fracking tests are conducted at 10 MPa confining pressure, with vertical compressive loading, as well as two horizontal stresses that simulate reservoir triaxial stress state. Multiple injection scenarios are tested to investigate the effect of the pore fluid injection conditions on the fracking and failure mechanisms. In-situ micro-seismic monitoring via eight acoustic emissions sensors is used for logging the fracking events evolution with time. Post-experimental characterization included computational tomography (CT) scanning to characterize the resulting fracture patterns.

## 1 Introduction

A precise understanding of the hydraulic fracturing (HF) mechanisms is of vital importance to maximize oil/gas recovery from tight reservoirs. Lab-scale HF serves as an attractive solution to understand the underlying physics of the HF process and its controlling parameters. Experimental shreds of evidence on the effect of pore pressure on tensile fractures are well known in literature [1–4], as well as the role of the effective confining pressure in augmenting the tensile strength of porous rocks [5]. This work presents HF experiments at triaxial stress state of Berea sandstone (BST) at different injection conditions. The purpose is to improve the understanding of the tensile failure and HF mechanism that is activated via the applied pore pressure. Post-experimental characterization included micro-computed tomography (CT) scanning of the produced fracking surface. The effect of the pore fluid viscosity and its injection rate on the pore pressure evolution and the related HF mechanisms are explored.

## 2 Experimental Setup

### 2.1 General description

The experimental apparatus used in this work is Autolab3000, which is capable of reproducing in-lab reservoir conditions to perform triaxial cyclic or monotonic compression tests [6]. The original design has been enhanced to include a HF cell where controlled triaxial stress states can be applied in addition to the

injection of selected fracking fluid. The tested samples are cylindrical cores that can have a diameter of up to 100 mm. Autolab3000 consists of three units, among which the confining vessel is the most essential where the samples are loaded and tested. The second unit is the pressure intensification unit that can provide up to 140 MPa. In-situ micro-seismic monitoring via eight acoustic emissions sensors is used for logging the induced microseismic events.

### 2.2 Sample configuration

In the present work, HF experiments are conducted on samples of 88 mm diameter and 90 mm height. Figure 1 (a) represents schematically the side view of the sample configuration, where the required drilling for the tube fixation and the pore hole is illustrated. This sample configuration is a result of an experimental optimization that has been done prior to the present experiments, which increased the quality of sample preparation that reduces related experimental errors. The injection tube is fixed inside the drilling hole of 14-mm diameter via 3M Scotch-Weld 2216 epoxy adhesive. Two 3D printed fittings are used to eliminate excess epoxy flow inside the pore hole, and to make the tube and the drilled hole co-axial. The pore hole is centered on the sample height, which allows an efficient injection pressure application through the injected fracking fluid.

\* Corresponding author: [rashid.abualrub@ku.ac.ae](mailto:rashid.abualrub@ku.ac.ae), [rashedkamel@yahoo.com](mailto:rashedkamel@yahoo.com)

### 2.3 Material used

BST has been selected to conduct the presented HF tests. The unconfined compressive strength and Young's modulus of BST are 69 MPa and 24.8 GPa, respectively [6]. Confined and unconfined compressive tests were conducted in previous work on this rock to characterize its mechanical properties as well as the plasticity and damage evolution at different confining pressure levels [6].

### 2.4 Loading conditions

The current experimental setup is capable of reproducing reservoir conditions, where the confining pressure ( $\sigma_h$ ) can be up to 138 MPa. In addition to this, two other loading components can be applied to the sample as shown in Figure 1 (a); namely: the major horizontal stress ( $\sigma_H$ ), as well as the axial load ( $\sigma_{ax}$ ).

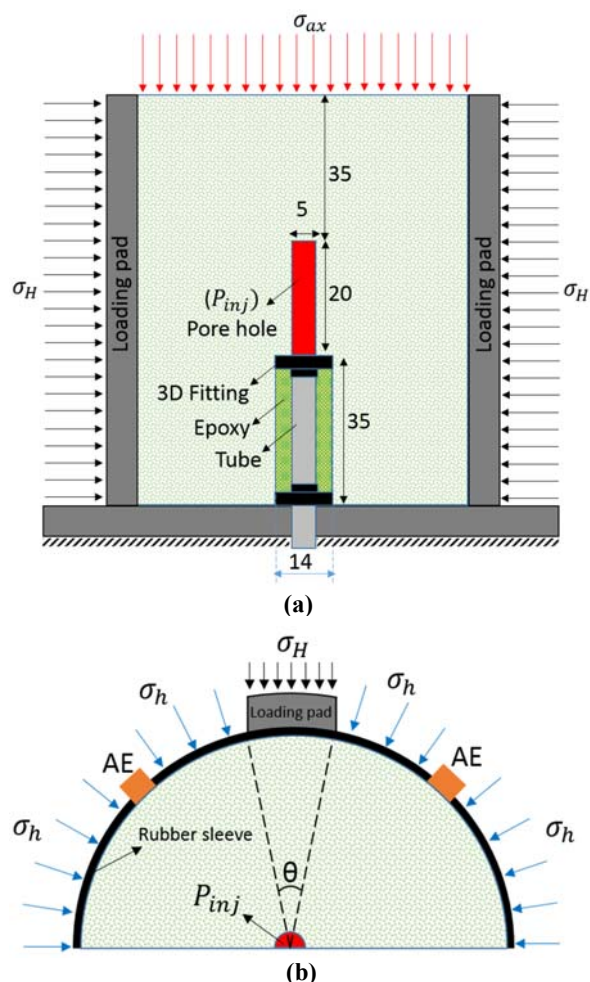


**Figure 1:** The optimized sample configuration, loading condition, and tube fixation with dimensions in [mm], as seen in (a) front view (b) half of the mid-height cross-section view.

A curved metallic loading pad is actuated hydraulically to apply the required value of  $\sigma_H$  over a defined area of the sample corresponding to  $\theta = 20^\circ$ , as shown in Figure 1(b). The sample is loaded inside a rubber sleeve that contains

eight acoustic emission sensors and the two metallic loading pads.

### 2.5 Conducted tests

**Porosity and permeability:** Three 38 mm-diameter cores of 76 mm height were tested for their permeability and porosity. The permeability tests were conducted at 2.75 MPa confinement, with a Nitrogen gas flow rate of 14 cc/min while ( $P_{Inlet} - P_{Outlet}$ ) was maintained at 6.9 kPa.

On the other hand, the porosity tests were made using digital modular Helium expansion volume meter.

**Brazilian tests:** For the prepared fracking sample as in Figure 1 (a), two Brazilian tests were performed on the subject rock at 10 MPa confining pressure, and three other tests were done at unconfined conditions. In these tests,  $\sigma_H$  was monotonically increased till the sample failure at  $\sigma_{H(Braz)}$ .

**Fracking experiments:** The fracking experiments presented here were performed at  $\sigma_h$  10 MPa,  $\sigma_H$  of 112 MPa, and  $\sigma_{ax}$  of 16 MPa. Investigation of the bedding effect of HF of BST has been conducted in previous work [7]. Thus, in all of the Brazilian and HF tests presented in the present work  $\sigma_H$  was applied perpendicular to the bedding planes. After the boundary conditions are applied, the fracking fluid injection is introduced. In the presented experiments, two fracking fluids are used, namely: oil MultiTherm PG-1 and Glycerin. Table 1 lists the conducted tests along with fracking fluid injection details, where (H) refers to periods where the injection is held, and the different steps are separated by a comma.

**Table 1 :** Details of the fracking fluid injection

Test	Injection	(Rate) [cc.min <sup>-1</sup> ]/(Duration) [s]
T1	Oil	(40)/ until failure
T2	Oil	(40)/ until failure
T3	Oil	(20)/(45), H/(15), (20)/(45), H/(15), (40)/(22), H/(15), (40)/(22)
T4	Oil	(400)/ until failure
T5	Glycerin	(10)/ until failure
T6	Glycerin	(20)/(123), H/(117), (45)/(66), H
T7	Glycerin	(40)/ until failure

## 2 Results and observations

### 2.1 Permeability and porosity tests

The permeability measurement revealed an average of  $(25.3 \pm 6)$  mD, which indicates a huge variation of permeability from one core to another. However, the porosity measurements were more consistent with an average of  $(14.9 \pm 0.3)$  % by volume.

## 2.2 Brazilian tests

The Brazilian tests at 10 MPa confinement resulted in sample failure at  $\sigma_{H(Braz)}$  ( $248 \pm 1.3$ ) MPa as an average of the failure points obtained from both tests. On the other hand, the unconfined Brazilian tests failed at  $\sigma_{H(Braz)}$  ( $87.5 \pm 9.8$ ) MPa as an average of the three tests.

## 2.3 Results of the fracking tests

In these HF tests, the applied  $\sigma_H$  is around 45% of  $\sigma_{H(Braz)}$  that was obtained at 10 MPa confinement pressure. This guarantees that the sample fails in the HF test due to the injected fluid and not due to the major horizontal stress ( $\sigma_H$ ). All samples were fracked successfully, where Figure 2 presents the evolutions of the injection pressure as a function of the injected volume.

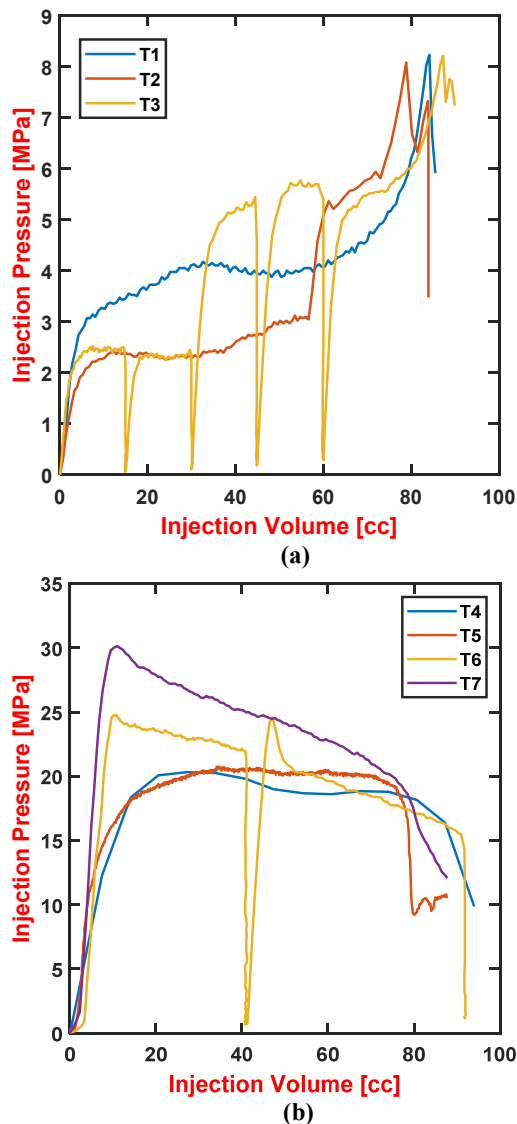


**Figure 2:** The evolution of the injection pressure as a function of the injected volume during the HF tests (a) T1-T3, and (b) T4-T7.

The obtained fracking planes are given in Figure 3, which shows that the cracks, in general, followed the direction of  $\sigma_H$  (triangular markers), while crack diverged close to the edges of loading pads. The post-experimental CT scan of T2 is provided at different sections in Figure 4.

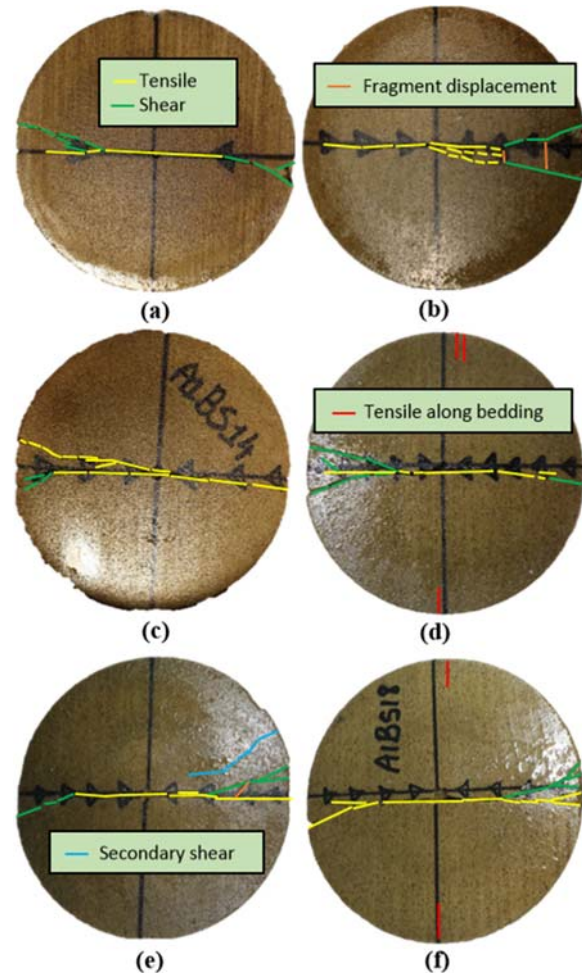


**Figure 3:** The fracked samples as seen on the top surface of (a) T1, (b) T2, (c) T4, (d) T5, (e) T6, and (f) T7.

## 3 Discussion and Conclusions

### 3.1 Regions of pressure evolution

The pressure evolution curves in Figure 2 (a), show some common features. These are better understood with the aid of Figure 5, which gives the microseismic events as recorded by the AE sensors for selected HF tests. The following description will take T1 data in Figure 5 (a) to describe the related phenomena. The initial highlighted zone represents a steep pressurization rate, which is due to the resistance that the porous rock demonstrates against the diffusion of the injected oil. At a critical value, the pressure gets high enough to overcome this resistance, which might start deforming the rock matrix causing microfractures, as indicated by the high AE counts by

arrow (1) in Figure 5 (a). The microseismic events corresponding to arrow (1) in Figure 5 (a) represents an inflection point, after which the pressurization rate reduces, such as indicated by arrow (2). Based on this, any AE counts in T1 higher than that indicated by arrow (1) in Figure 5 (a) represent serious microseismic events taking place.

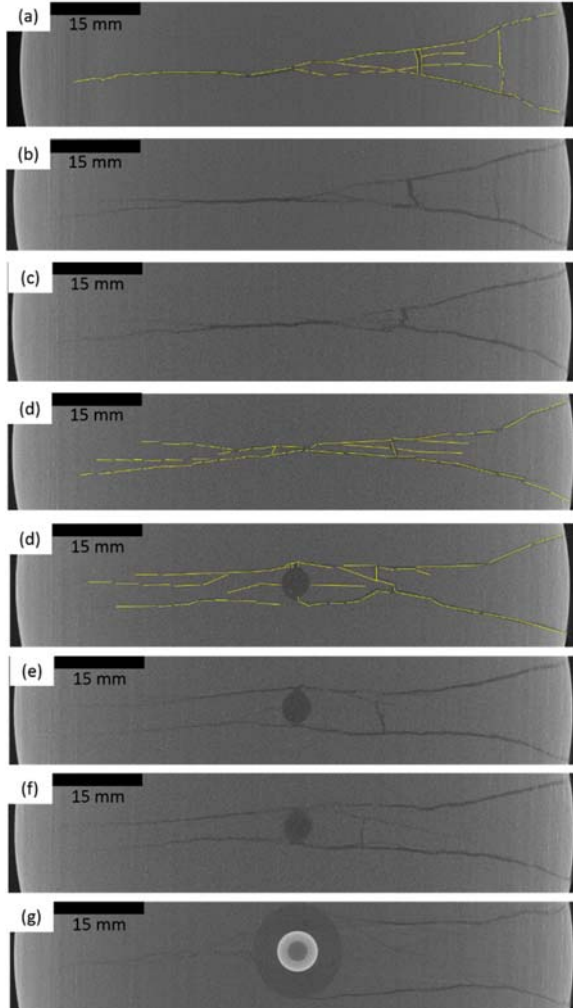
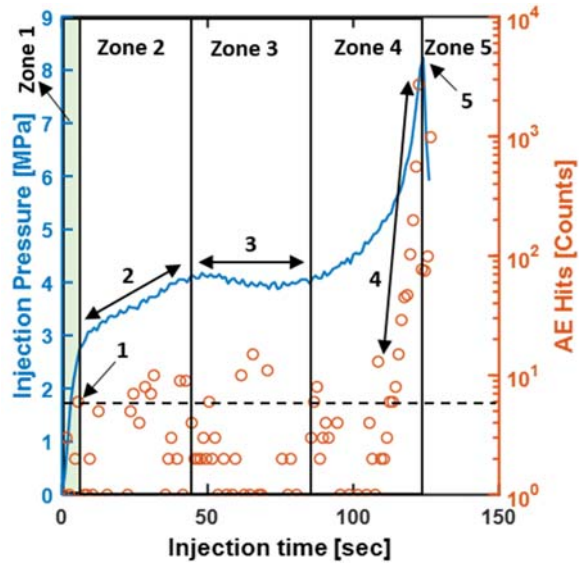
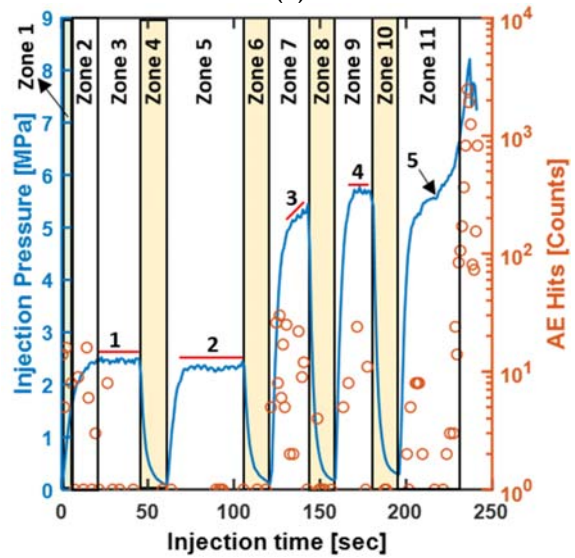


**Figure 4:** Computational tomography equidistant sections (a-g) of the upper part of fracking sample of T2.

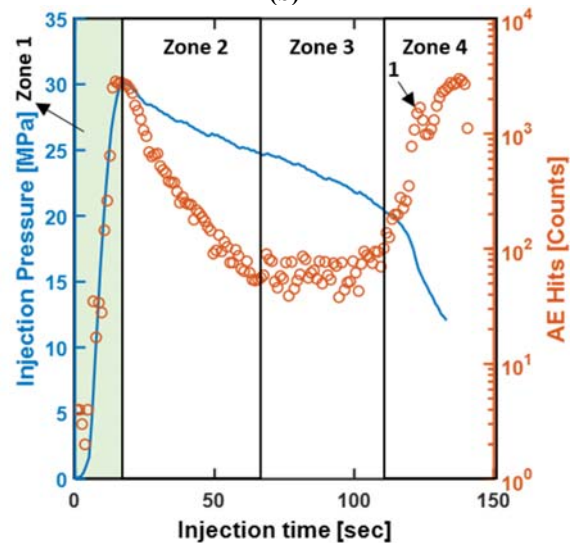
It can be noticed that zone 2 included more deformations as marked by the accompanied AE events there, leading to a pressure plateau in zone 3 as indicated by arrow (3). This indicates having reached enough permanent deformation of the rock matrix as an effect of the pore fluid, including by microcracks initiations and propagation. This increases the diffusion area between the fracking fluid and the rock matrix which, as an effect, leads to more or less a steady flow in zone 3, which remains the case until the pore volume gets almost saturated at around 80 cc of injection volume at the end of zone 3. These results are in agreement with the measured porosity of the tested rock which is about 15% by volume. The pressurization rate starts to increase steeply in zone 4 accompanied by a rapid increase of AE counts, indicated by arrow (4) until the failure of the sample at the point indicated by arrow (5).



(a)



(b)



(c)

**Figure 5:** The time log of AE counts during the HF tests (a) T1, (b) T3, and (c) T7.

### 3.2 Fracking planes and directions

The produced fracking planes were more or less aligned to  $\sigma_H$  at the central part of the sample as marked by the yellow tracing lines in Figure 3. These tensile cracks are caused by the augmentation of the pore pressure which reduces the effective confining pressure, leading to material weakening and failure. As an effect of the stress concentrations resulting from  $\sigma_H$  application, these cracks diverge later as marked by the green lines towards the stress concentration locations close to the edges of the lateral loading pads. After the samples are cracked, the sides holding  $\sigma_H$  become unsupported from the center of the sample, leading these wedges to collapse by the secondary cracks that are marked in green. Further cracks are generated within these wedges as an effect of  $\sigma_H$  compression and the caused sudden displacement of the resulting rock fragments, such as the orange lines in Figure 3. This effect can extend to the surrounding regions such as that shown by the blue lines in Figure 3 (e). When glycerine was used as the fracking fluid, the isolated cracks marked by the red lines in Figure 3 (d & f) were detected which correlates with bedding planes and extends along with the sample height. As side cracks are not directly caused by the pore pressure, it is believed that the cracks marked in green and blue are shear cracks resulting from the compression provided by the loading pads.

### 3.3 Reproducibility and the margin of error

The reproducibility was tested through T1 and T2, which were fracked at identical loading and injection conditions, yet their pressure evolution curves were quite distinct. This is partially ascribed to the huge variance of permeability that the tested cores have, which, as a consequence, will allow the injected oil to diffuse easier in the cases of higher permeability. On the other hand, this can be due to the variations of the crack initiation points from one sample to another due to their natural diversity of the local microstructure around the injection area. The obtained fracking planes in both tests are also not identical. The cracks obtained in T2 seemed to be much more complex, for which micro computational tomography scanning was made. The results are shown in Figure 4 by equally distant sections showing that the upper sections (a-c) had a simple cracking network as compared to the lower sections (d-g) where tensile and shear cracks alternated.

### 3.4 Cyclic injection of fracking fluid

The cyclic fracking test (T3) revealed new features about the fluid-solid interaction that were not detected in monotonic HF tests. The AE counts of the microseismic events given in Figure 5 (b) in zone 1-3 show features that are similar to what was discussed for zone 1-3 of the monotonic HF of T1 in Figure 5 (a). However, it was interesting that holding the injection in zone 4 and injecting again in zone 5 reproduced almost the same

pressure evolution of zone 1-3. Nevertheless, the new injection (zone 5) did not cause any remarkable AE events as the rock matrix has already been deformed and cracked up to this level of fluid interaction in the injection period of zone 1-3. However, the transition to pressure plateau (2) is obtained faster than that in zone 3. Doubling the injection rate after holding in zone 6 produced a new pressure transition period similar to that obtained in zone 2 with remarkable microseismic events recorded by the AE counts. This corresponds to the new deformation that the rock matrix undergoes, corresponding to the higher friction resulting from increasing the injection rate in this zone as compared to the previous ones. The injection in zone 9 is accompanied by more AE events leading to the pressure plateau (4) that was not yet obtained in zone 7 as marked by the slope (3). Point (5) represents 80 cc of injection, after which rapid pore pressure builds up, leading eventually to sample failure. This experiment revealed how the fracking fluid interacts with the rock matrix, and the features related to injecting a partially saturated porous rock.

### 3.5 Effect pore fluid viscosity on fracking

The HF tests T1 and T2 were performed at the same injection rate of test T7, yet their pressure evolutions were different in features and order of magnitudes. Here, the higher value of injection pressure obtained in the case of T7 is expected due to the higher friction associated with the higher viscosity of glycerine in T7 as compared to that of oil in T1-T2. The same applies to the difference between T3 and T6 for their first injection periods. Figure 5 (c) shows the time log of the microseismic events of T7 during the different zones of the HF test, which will be compared to T1-T3 in the following. It's noticed that the initial steep pressurization period marked by zone 1 is longer for T7 than the other two tests. It is accompanied by a higher number of AE counts that progressively increased until the breakup point at the end of zone 1. After this point, the slope of the pressure curve suddenly changes to almost a constant negative value over zone 2-3. The AE counts reveal an exponential decay (linear on the logarithmic scale) during zone 2, which expresses a quick relaxation of the rock matrix after each crack propagation taking place in this period. This AE behavior indicates a decaying crack propagation speed taking place in zone 2. Later, the number of counts gets stable with time in zone 3, which indicates almost a fixed amount of rock deformation and cracking with each new increment of the injected fluid. At the beginning of zone 4, the sample is saturated with the injection fluid, which reduces the effective confining pressure causing an exponential increase of the microseismic events leading to the total sample failure. The pressure evolution features of T6 before holding the injection was similar to that witnessed in T7. However, T7 had a higher pressure build up in the initial pressurization (zone1) due to the higher injection rate used in that test. The presented results are in agreement with the literature on the effect of viscosity and injection rate on HF [1-4].

### 3.6 Role of fluid diffusion and saturation in HF

Fracking at an injection rate of 10 cc/min in T5 caused the breakup pressure to be lower than that in both T6 and T7, as shown in Figure 2 (b). Injection at this slower rate gave the increment of injected fluid more time to diffuse into the porous network and the initiated cracks, leading to pore pressure relaxation before the next fluid increment arrives. After the initial steep pressurization in T5, a pressure plateau was obtained, a feature that is physically similar to what was explained earlier for T1-T3. The rock fails completely at ~80 cc of injected volume as marked by the pressure drop, which corresponds to the saturation of the sample. An identical phenomenological behavior to T5 is obtained when oil was used as the injection fluid at 400 cc/min in T4; as the associated friction augmented by increasing the flow rate compared to T1-T3. In both T4 and T5, the pore fluid didn't increase at the final sample failure point at around 80 cc of injection volume, unlike T1-T3. It's noticed that in tests T1-T3, the sample eventually fails at a common injection pressure of ~8 MPa, which comes after the saturation point. This is ascribed to the reduction of the effective confining pressure, which reduces the tensile strength of the rock, leading to failure at a critical effective pressure value. This failure mechanism is the opposite of the strengthening mechanism by the confining pressure that was witnessed for the confined Brazilian tests as compared to unconfined tests presented in this work. For T4-T7, the injection pressure was already higher than the confining pressure at the obtained pressure plateau, yet failure took place only after saturation was obtained.

### 3.7 Role of localized pore pressure in HF

An early failure mechanism is manifested in tests T6-7 due to the energetic tensile cracking resulting from the localized pore pressure at the end of the initial pressurization period. This is confirmed by the first AE counts recorded in Figure 5 (c) for T7 as an example of what's happening in T6-T7, while the second peak represents a failure by the second mechanism after the saturation point. The limited diffusion of glycerine under the higher injection pressure in T7 and T6 during the initial pressurization led to higher localized tensile stress generation as compared to T1-T5, where diffusion was easier. The inflection of the pressurization rate after the resulting tensile failure in T6-7 indicates an intensive tensile fracture, as witnessed by the AE counts at the end of zone 1 in Figure 5 (c). This behavior is more pronounced at high pore fluid viscosity and/or high injection rate, such as in T4-T7, yet it's the same mechanism of failure observed at the end of zone 1 in T1-T3 which had lower intensities. This difference in intensity is seen by the AE counts in Figure 5 at the end of zone 1 of each case. In contrast, the intensity of the second failure obtained after sample saturation was comparable for the different tests regardless of the injected fluid, as seen in Figure 5. These observations emphasize the role of localized fluid-solid interaction and friction for the first failure mechanism. On the other hand, the role of the pore pressure augmentation leading to

confining pressure reduction is the main actor for the second failure mechanism near the rock saturation.

**Acknowledgment:** The authors acknowledge the financial support provided by Abu Dhabi National Oil Company (ADNOC) through Contract NO. 16282.01.

### References

- [1] M.S. Bruno, F.M. Nakagawa, Bore pressure influence on tensile fracture propagation in sedimentary rock, *Int. J. Rock Mech. Min. Sci.* 28 (1991) 261–273. doi:10.1016/0148-9062(91)90593-B.
- [2] C. Baptista-Pereira, B. Gonçalves da Silva, Effects of fluid diffusivity on hydraulic fracturing processes using visual analysis, in: *Am. Rock Mech. Assoc.*, 2019.
- [3] Y. Wang, D. Zhang, Y.Z. Hu, Laboratory Investigation of the Effect of Injection Rate on Hydraulic Fracturing Performance in Artificial Transversely Laminated Rock Using 3D Laser Scanning, *Geotech. Geol. Eng.* 37 (2019) 2121–2133. doi:10.1007/s10706-018-0749-7.
- [4] L. Zhuang, K.Y. Kim, S.G. Jung, M. Diaz, K.B. Min, Effect of Water Infiltration, Injection Rate and Anisotropy on Hydraulic Fracturing Behavior of Granite, *Rock Mech. Rock Eng.* 52 (2019) 575–589. doi:10.1007/s00603-018-1431-3.
- [5] L. Yawei, A. Ghassemi, Rock Failure Behavior and Brittleness under the Confined Brazilian Test, in: *ARMA18 - 52nd US Rock Mech. / Geomech. Symp.*, American Rock Mechanics Association, Seattle, Washington, 2018. <https://www.onepetro.org/conference-paper/ARMA-2018-897>.
- [6] H. Mubarak, R.P. Saji, R. Zhu, R.L. Sousa, M. Sassi, R.K. Abu Al-Rub, Plasticity and damage analysis of Berea sandstone via cyclic triaxial loading under high confinement pressure, *53rd U.S. Rock Mech. Symp.* (2019).
- [7] G.L. Zhu, R.P. Saji, H. Mubarak, R.L. Sousa, M. Sassi, R.K. Abu Al-Rub, Experimental and numerical investigation of hydraulic fracturing under reservoir conditions, *53rd U.S. Rock Mech. Symp.* (2019).